On Quantitative Errors of Two Simplified Unsteady Models for Simulating Unidirectional Nonlinear Random Waves on Large Scale in Deep Sea

Jinghua Wang[1], Q.W. Ma[1,a)] and Shiqiang Yan[1]

[1]School of Mathematics, Computer Science and Engineering, City, University of London, London, EC1V 0HB, UK

To investigate nonlinear random wave dynamics or statistics, direct phase-resolved numerical simulation of nonlinear random waves in deep sea on large-spatial and long-temporal scales are often performed by using simplified numerical models, such as these based on the Nonlinear Schrödinger Equation (NLSE). They are efficient and can give sufficiently acceptable results in many cases but they are derived by assuming narrow bandwidth and small steepness. So far, there has been no formula to precisely predict the quantitative errors of such simplified models. This paper will present such formulas for estimating the errors of Enhanced NLSE based on Fourier transform and Quasi Spectral Boundary Integral (QSBI) method when they are applied to simulate ocean waves on large-spatial and long-temporal scales (about 128 peak wave lengths and 1000 peak periods). These formulas are derived by fitting the errors of the simplified models, which are estimated by comparing their wave elevations with these obtained by using a fully nonlinear model for simulating the cases with initial conditions defined by two commonly-used ocean wave spectra with a wide range of parameters. Based on them, the suitable regions for the simplified models to be used are shown.

1 INTRODUCTION

It is now increasingly recognized that direct and accurate simulation of ocean waves considering sufficient nonlinearity is necessary for understanding their dynamics. The simulation is challenging, not only due to the randomness and nonlinear effects of ocean waves, but also the fact that it needs to be carried out in a quite large scale and for a long duration[1].

To do that, phase-averaged models, such as WAM, WAVEWATCH and SWAN etc., are very popular[2-4]. The models are based on linear wave energy transportation equation with all nonlinear effects modelled by empirical source terms. They give the approximated evolution of wave spectra and wave statistical parameters such as significant wave height. A great success has been achieved using these models, so that we all benefit from the forecast of the wave statistics provided by, e.g, ECMWF, NOAA and Met Office UK. Nevertheless, in many applications and situations, one requires more specific and accurate information rather than just wave statistics such as direct velocity fields, acceleration fields and wave slopes of nonlinear ocean waves to gain better understanding of random waves dynamics. To achieve such goals, phase-resolved models should be employed[1,5]. In this class of models, the dynamic equations governing the velocity and wave elevation are directly solved in time domain and so such information becomes available throughout the space at all time steps. Among them, numerical models based on the Navier-Stokes (short as NS) equation or coupled potential & NS model[6,7] may be employed but they are computationally prohibitive for large scale simulations. Nevertheless, the models based on nonlinear potential theory alone are much faster, and thus a brief review is given below.

One class of such models are fully nonlinear potential methods based on Finite Difference Method[8-10],

a) Author to whom correspondence should be addressed. Electronic mail:Q.Ma@city.ac.uk

Boundary Element Method[11,12], and Finite Element Method[13,14] or Quasi Arbitrary Lagrangian-Eulerian Finite Element Method[15,16]. However, they are still computationally expensive for very large scale simulations, thus barely applied so far to model waves in a scale of hundred wave lengths for thousand wave periods.

Another class of nonlinear models are these based on or associated with use of the Fast Fourier Transform (FFT), such as FFT mixed global minimizing approach[17], FFT mixed lower-upper matrix decomposition method[18] and FFT mixed finite difference scheme[19], Spectral Continuation method[20-22], Irrotational Green-Naghdi model[23], Higher-Order Spectral (HOS) method[24,25], Spectral Boundary Integral method[26-28] and Enhanced Spectral Boundary Integral (ESBI) method[29]. This class of models is relatively faster but still needs significant amount of time. For an example, a 3D random sea simulation covering 42×42 peak wave lengths for 250 peak wave periods takes 10 CPU days on a 3 GHz-Xeon single processor PC by using the HOS method[30].

To be more efficient, researchers have developed many simplified potential models. One group of the models is the second order wave models, but Kriebel[31,32] indicated that they could not describe the continuous spectral energy transfer between wave components as the amplitude of each wave component was independent of time, and thus they were only sufficiently accurate when the wave steepness was quite small (i.e., when the energy transfer between wave components was insignificant). The other group is the shallow water models, i.e., Boussinesq and KdV equations[33,34], including the higher order versions[35-37]. They are suitable for weakly nonlinear shallow water waves[38,39], thus will not be further discussed as this paper focuses only on the waves in deep seas.

Another class of simplified models for simulating waves in deep seas are these based on the Zakharov equation[40-42] or nonlinear Schrödinger equation (shortened as NLSE)[40-44]. The NLSE has a number of different versions, such as the cubic NLSE (shortened as CNLSE)[40-44], the NLSE using the Dysthe equation[45,46], the Modified NLSE (shortened as MNLSE)[47], the Enhanced NLSE (shortened as ENLSE-4)[48], the Higher-Order Dysthe equation in terms of the Hilbert transform (shortened as ENLSE-5H)[49], the Enhanced NLSE based on Fourier transform (shortened as ENLSE-5F)[50] and the Hamiltonian higher-order NLSE[78-80]. These methods are based on the assumption that the bandwidth of random waves is narrow. In addition, Wang, *et al*.[50] suggested a simplified method called QSBI (Quasi Spectral Boundary Integral) method, which is obtained from simplifying the fully nonlinear ESBI method[29] by only keeping the convolution terms up to the third order while ignoring the integration terms for evaluating the vertical velocity. This method can be applied to simulate random waves without limitation on bandwidth.

Applications of NLSE models to the direct simulation of random seas on large-spatial and long-temporal scales are extensive. For example, Onorato, *et al*.[51] employed the CNLSE and performed more than 300 simulations of random sea states on a scale of 100 peak wave lengths (L_0) and 25 peak periods (T_0), and found that rogue waves are more likely to occur when the initial wave steepness is large. Dysthe, *et al*.[52] studied the evolution of the wave spectra based on both the CNLSE and the ENLSE-4 in a domain covering $100L_0\times100L_0$ for $150T_0$, and found a power law behavior $k^{-2.5}$ for integrated spectra[53]. Later, Dysthe, *et al*.[54] and Socquet-Juglard, *et al*.[55] simulated 3D random seas covering $128L_0\times128\ L_0$ for $150T_0$ based on the ENLSE-4, and pointed out that the probability density of surface elevation fits the Tayfun distribution very well. In addition, Shemer, *et al*.[56] studied the probability of rogue waves in a domain of 77 L_0 for $100T_0$ based on both the CNLSE and the Dysthe equation, and pointed out that the probability of rogue waves reaches the highest when the local bandwidth attains the maximum. Subsequently, Onorato, *et al*.[57] brought the effects of current into the CNLSE and showed that rogue waves can be triggered naturally when a stable wave train enters a region of an opposing current flow field, based on a numerical simulation in a domain of 60 L_0 for period of 60 T_0. Later, Ruban[58] considered the effects of non-uniform current on random waves based on the CNLSE, and simulated the wave field spanning 400

L_0 for 1000 T_0. It is concluded that the reason of rogue wave occurrence is because of the interaction of quasi-soliton coherent structures. Meanwhile, Zeng & Trulsen[59] developed a NLSE for uneven bottom to simulate random waves propagating over $143L_0$ for 159 T_0, and indicated that a change of water depth can provoke a spatially non-uniform distribution of kurtosis on the lee side of the slope. More recently, Sergeeva, *et al*.[60] simulated random waves in coastal regions on a scale of 20~40 L_0 for up to 80 T_0 based on a variable CNLSE, and found that rogue waves are likely to occur at deeper locations. Taklo, *et al*.[61] also simulated a random sea on a scale of $70L_0$ for $400T_0$ based on the Zakharov equation and found that the measured dispersion relation deviates from the linear dispersion relation when the bandwidth is sufficiently narrow. Adcock, *et al*.[62] recently applied the MNLSE to simulate random waves spanning $22L_0 \times 22$ L_0 for 300 T_0 and suggested that the nonlinearity can give a small amount of extra elevation above that of linear theory, but the nonlinear dynamics does change the shape and structure of extreme waves. Moreover, Simanesew, *et al*.[63] used the MNLSE to simulate random waves covering $100L_0 \times 100$ L_0 for $200T_0$ and compared with laboratory results, then suggested that a strong frequency-dependence of the directional spread will develop due to nonlinear effects. Zhang, *et al*.[64] also employed the MNLSE to simulate random waves on the scale of $256L_0 \times 256L_0$ for 60 T_0, and found that the statistical properties of the simulated wave fields are basically consistent with the laboratory observation. Clamond, *et al*.[65] carried out a long time simulation of soliton evolution by using the CNLSE, ENLSE-4 and their fully nonlinear method. They demonstrated that the ENLSE-4 model was more accurate than the CNLSE by showing that the results of the CNLSE started to become notably different from the results of their fully nonlinear method at 100 periods while these from ENLSE-4 were almost the same as those of the fully nonlinear method even at 150 periods. Wang[66] confirmed the observation of Clamond, *et al*.[65] and indicated that the results of the ENLSE-5F model is correlated well with the fully nonlinear results at 500 periods when the results of ENLSE-4 became quite different from the latter. The additional tests (not presented here) carried out by Wang[66] also show that the MNLSE and ENLSE-4 models give almost the same results and are more accurate than the CNLSE and other lower order NLSE models, but less accurate than the ENLSE-5F in long time simulations. The QSBI method has just been proposed and only applied as an alternative for the NLSE in the hybrid model of Wang, *et al*.[50]. That paper just demonstrates that the QSBI method is generally more accurate than the ENLSE-5F model but takes more computational time.

Although these simplified models are computationally efficient, they are accurate in limited conditions. Dysthe, *et al*.[52] had pointed out that for narrow bandwidth waves the CNLSE and MNLSE is reliable only when a dimensionless time scale (the time multiplied by peak circular frequency) is up to $2\varepsilon^{-2}$ and $10\varepsilon^{-2}$ (ε peak wave number times amplitude), respectively. This information is very useful but it does not tell what is the specific values of errors if the models are employed. Xiao[67] compared the results obtained by their HOS method and two NLS-type methods (MNLSE and NLSE using the Dysthe equation), and showed that the NLS-type methods could produce similar results to the HOS method when the spectrum change is slow, otherwise the results of NLS-type methods might be significantly different from those of the HOS method. It is desired that one would quantitatively estimate the errors of the simplified methods when applying them to simulate the random waves. According to the latest literature, the way to quantitatively and precisely estimate their errors seems not to be available, at least in public domain.

The main purpose of this paper is to bridge the gap and present a method for estimating the quantitative error of Enhanced NLSE based on Fourier transform (ENLSE-5F) when it is applied to simulate ocean waves in large-spatial and long-temporal scales, such as 128 peak wave lengths and 1000 peak periods. Along with this, the paper will also quantify the errors of the QSBI method and the linear model. The reason for concerning about the QSBI is that when the ENLSE-5F cannot be used, one may use the QSBI as an alternative. The reason for concerning

about the linear model is because it is often employed in practice and it would be useful to know its errors.

2 METHEDOLOGIES

In order to obtain the quantitative errors, the fully nonlinear method (ESBI) and the simplified models will be applied to simulate a large number of cases, whose initial conditions are defined by two different but commonly-used ocean wave spectra with a wide range of wave parameters. For each of the cases, the errors of the simplified models are estimated by comparing their wave elevations with these obtained by using the ESBI at the end of the simulation. After the errors of all cases are obtained, the formulas are formulated by using a data fitting technique.

All the numerical models have been documented in the publications cited above. Their formulations will only be briefed for completeness in the following sections. For convenience, all the variables involved will be non-dimensionalised in a consistent way, e.g., the length variables multiplied by peak wave number k_0, and the time variables multiplied by peak circular frequency ω_0, where $\omega_0 = \sqrt{gk_0}$ and g the gravity acceleration. All the dimensionless variables are listed in Table I.

A. The ESBI and QSBI

The Spectral Boundary Integral (SBI) method has been suggested by Clamond & Grue[26], Fructus *et al*.[68] and Grue[28]. It was improved and named as the ESBI by Wang & Ma[29] and Wang *et al*[50]. This method is based on the potential theory with the boundary conditions on the free surface formulated as the skew-symmetric prognostic equation

$$\frac{\partial \boldsymbol{M}}{\partial T} + \boldsymbol{\Lambda M} = \boldsymbol{N} \tag{1}$$

where

$$\boldsymbol{M} = \begin{pmatrix} KF\{\eta\} \\ K\Omega F\{\tilde{\phi}\} \end{pmatrix}, \boldsymbol{\Lambda} = \begin{bmatrix} 0 & -\Omega \\ \Omega & 0 \end{bmatrix}, \boldsymbol{N} = \begin{pmatrix} K\left(F\{V\} - KF\{\tilde{\phi}\}\right) \\ K\Omega F\left\{\frac{1}{2}\left[\frac{(V+\nabla\eta\cdot\nabla\tilde{\phi})^2}{1+|\nabla\eta|^2} - |\nabla\tilde{\phi}|^2\right]\right\} \end{pmatrix} \tag{2}$$

where η and $\tilde{\phi}$ are the dimensionless free surface elevation and the velocity potential on the free surface, respectively, as shown in Table I that also includes the definition of other dimensionless variables; V is the dimensionless vertical velocity defined by $V = \partial\phi/\partial n\sqrt{1+|\nabla\eta|^2}$, Ω is the dimensionless frequency defined by $\Omega = \sqrt{K}$ with $K = |(\kappa, \zeta)| = \sqrt{\kappa^2 + \zeta^2}$. In the above equations, the Fourier transform $F\{\ \}$ and the inverse transform $F^{-1}\{\ \}$ are given by

$$\hat{\eta}(\boldsymbol{K}, T) = F\{\eta\} = \int_{-\infty}^{\infty} \eta(\boldsymbol{X}, T) e^{-i\boldsymbol{K}\cdot\boldsymbol{X}} d\boldsymbol{X} \tag{3}$$

$$\eta(\boldsymbol{X}, T) = F^{-1}\{\hat{\eta}\} = \frac{1}{4\pi^2}\int_{-\infty}^{\infty} \hat{\eta}(\boldsymbol{K}, T) e^{i\boldsymbol{K}\cdot\boldsymbol{X}} d\boldsymbol{K} \tag{4}$$

The solution for Eq.(1) is expressed by

$$\boldsymbol{M}(T) = e^{-\boldsymbol{\Lambda}(T-T_0)} \int_{T_0}^{T} e^{\boldsymbol{\Lambda}(T-T_0)} \boldsymbol{N} dT + e^{-\boldsymbol{\Lambda}(T-T_0)} \boldsymbol{M}(T_0) \tag{5}$$

where

$$e^{\Lambda\Delta T} = \begin{bmatrix} \cos\Omega\Delta T & -\sin\Omega\Delta T \\ \sin\Omega\Delta T & \cos\Omega\Delta T \end{bmatrix} \tag{6}$$

The vertical velocity V can be split into four parts, i.e., $V = V_1 + V_2 + V_3 + V_4$ (see Eqs. (B.1)~(B.4) in APPENDIX B). In the study of Wang & Ma[29], several numerical techniques had been proposed in order to improve the computational efficiency. Firstly, they introduced a new numerical de-singularity technique to evaluate the integration parts more efficiently. Secondly, they reformulated the equations for V_3 and V_4 as (Eqs. (B.5)~(B.10) in APPENDIX B)

$$V_3 = V_{3,C} + V_{3,I} = \underbrace{V_3^{(1)}}_{4th} + \underbrace{V_3^{(2)}}_{6th} + \underbrace{V_{3,I}}_{integration} \tag{7}$$

$$V_4 = V_{4,C} + V_{4,I} = \underbrace{V_4^{(1)}}_{3rd} + \underbrace{V_4^{(2)}}_{5th} + \underbrace{V_4^{(3)}}_{7th} + \underbrace{V_{4,I}}_{integration} \tag{8}$$

During the simulation, the wave properties are examined. The integration parts are evaluated only when their effects are significant; otherwise they are neglected. In such a way, computational time is saved without degrading the accuracy of numerical results. Thirdly, they developed a new technique for anti-aliasing to eliminate aliasing problems associated with convolutions in the above equations.

The QSBI (Quasi Spectral Boundary Integral) method is a simplified form of the ESBI method suggested by Wang, *et al*.[50]. In this method, the velocity accounts only for the convolution terms up to the third order and neglecting the integration terms, i.e., $V = V_1 + V_2 + V_4^{(1)}$ with others being the same.

The ESBI model had been validated in different situation as described in Wang and Ma[29] and Wang, *et al*.[50], which showed the good accuracy of the method. One of the validated cases is summarized here. In this case, the ESBI is used for the simulation of a Stokes wave perturbed by a directional side-band wave $\delta\eta = 0.025\epsilon[sin(\boldsymbol{K_1}\cdot\boldsymbol{X}) + sin(\boldsymbol{K_2}\cdot\boldsymbol{X})]$, where $\epsilon = 0.2985$, $\boldsymbol{K_1} = (3/2, 4/3)$ and $\boldsymbol{K_2} = (3/2, -4/3)$. The computational domain covers 2×1.5 Stokes wave lengths on transversal and longitudinal direction and is resolved by $2^8\times2^8$ points. The duration of the simulation is 18 wave periods. For this case, Fructus, *et al*.[68] presented a quantitative result of the ratio $\Psi_\epsilon = |F\{\eta\}|_{(\boldsymbol{K}=(3/2,4/3),T)}/|F\{\eta\}|_{(\boldsymbol{K}=(1,0),T=0)}$, where $|F\{\eta\}|_{(\boldsymbol{K}=(3/2,4/3),T)}$ is the value of the spectral component at a time T corresponding to $\boldsymbol{K} = (3/2, 4/3)$. Their result is re-produced in FIG. 1. A code based on the method in Fructus, *et al*.[68] was also programmed, which is referred to as the Fructus method and used to compute the same case. Both results are compared with that from the ESBI in FIG. 1. It shows that the code for the ESBI produces almost the same result as the Fructus method and the error at the end of the simulation is about 0.2%. The robustness and accuracy of the ESBI model has also been shown by other publications[27,38,65].

B. The ENLSE-5F

As indicated above, there are many different forms of NLSE models. For the purpose of this paper, the ENLSE-5F model will be used. That is because of the following considerations. Compared with other lower order counterparts based on the Dysthe equation, this one is the most accurate but does not require significantly more computational time. Compared with Hamiltonian higher-order NLSEs[78-80], the ENLSE-5F model is chosen by considering the following factors. (i) This paper is concerned about methods for phase-resolved simulation of random waves which needs to look at the free surface (or wave) elevation. The envelope solved in the ENLSE-5F is directly related to the free surface elevation, and thus it is relatively easier to transform between the wave elevation and the envelope. The Hamiltonian NLSE is associated with the wave action which is nonlinearly related

to the wave elevation. This feature makes it relatively more difficult to transform between the free surface elevation and the wave action, in particular, from the wave elevation to the wave action. (ii) Detailed analysis (not presented in this paper) can show that the leading order of error of the ENLSE-5F is $\mu^3\varepsilon^3$ while that of Hamiltonian higher-order NLSEs presented by both Craig, et al.[79] and Gramstad & Trulsen[80] is $\mu^2\varepsilon^3$, where μ and ε denote the magnitude of the bandwidth and the wave steepness, respectively. One of the purposes of this paper is to quantify the error of NLSE and the boundary of suitability. From their orders of error, it can be seen that the error of ENLSE-5F would not be larger than that of Hamiltonian higher-order NLSEs and so its boundary of suitability should cover the boundary of suitability of Hamiltonian higher-order NLSEs. In other words, in the region where ENLSE-5F is not valid or not sufficiently accurate, Hamiltonian higher-order NLSEs should not be sufficiently accurate either. (iii) Although the NLSE equations based on the Dysthe equation, including ENLSE-5F may not theoretically guarantee the conservation of the Hamiltonian (total wave energy) in finite and shallow waters, the effect of the problem is not significant in deep water concerned about in this paper, as indicated by Craig, et al.[79]. Socquet-Juglard, et al.[55] showed numerically that the MNLSE conserved the total energy to high accuracy within the bandwidth constraint for the cases they considered. Tests have been carried out on the Hamiltonian estimated by using the ENLSE-5F for a typical case with strong nonlinearity considered in this paper, and the results (not presented here) demonstrated that the error of the Hamiltonian is less than 0.2% for the simulation up to 1000 peak periods. However, for the cases in finite and shallow water, Hamiltonian higher-order NLSEs may be better, which will be studied in future work.

The ENLSE-5F model was suggested by Debsarma & Das[49], and later modified by Wang, *et al.*[50]. In the method, the free surface elevation and velocity potential are written in the summation of several harmonics by introducing the envelope[45], i.e.,

$$\eta = \bar{\eta} + \frac{1}{2}\left(Ae^{i\theta} + A_2e^{2i\theta} + A_3e^{3i\theta} + c.c.\right) \tag{9}$$

$$\phi = \bar{\phi} + \frac{1}{2}\left[Be^{i\theta+Z} + B_2e^{2(i\theta+Z)} + B_3e^{3(i\theta+Z)} + c.c.\right] \tag{10}$$

where A and B are complex envelops of the first harmonic of free surface elevation and velocity potential respectively, A_2, A_3, B_2 and B_3 are the complex envelope coefficients of the high-order harmonics, $\bar{\eta}$ and $\bar{\phi}$ are slowly varying parts of free surface elevation and velocity potential[45], $c.c.$ represents the complex conjugate, and $\theta = X - T$. The envelop A satisfies the following equations

$$\begin{aligned}\frac{\partial A}{\partial T} + F^{-1}\{i(\omega-1)F\{A\}\} = &-\frac{i}{2}|A|^2A - \frac{3}{2}|A|^2\frac{\partial A}{\partial X} - \frac{1}{4}A^2\frac{\partial A^*}{\partial X} + \frac{i}{2}AF^{-1}\{|\kappa|F\{|A|^2\}\} + \\ &\frac{5i}{8}|A|^2\frac{\partial^2 A}{\partial X^2} + \frac{9i}{16}A^*\left(\frac{\partial A}{\partial X}\right)^2 + \frac{i}{8}A\frac{\partial A}{\partial X}\frac{\partial A^*}{\partial X} - \frac{i}{8}A^2\frac{\partial^2 A^*}{\partial X^2} + \frac{1}{2}\frac{\partial A}{\partial X}F^{-1}\{|\kappa|F\{|A|^2\}\} + \\ &\frac{1}{4}AF^{-1}\left\{|\kappa|F\left\{A\frac{\partial A^*}{\partial X}\right\}\right\} + \frac{1}{2}AF^{-1}\left\{|\kappa|F\left\{A^*\frac{\partial A}{\partial X}\right\}\right\} + \frac{i}{8}AF^{-1}\{\kappa^2F\{|A|^2\}\}\end{aligned} \tag{11}$$

The other parameters (A_2, A_3, B_2, B_3 $\bar{\eta}$ and $\bar{\phi}$) are estimated by using Eqs. (A.1)~(A.6) in APPENDIX A. The numerical code for the ENLSE-5F model has been validated in Wang, *et al.*[50] and Wang[66], which will not be repeated here.

3 NUMERICAL SIMULATIONS AND RESULTS

As indicated above, the errors of the simplified models will be quantified by finding the differences between their results and these of the fully nonlinear model. A short summary of all the models is presented in Table II, in

which the linear model is simply described by Eq. (14) below.

All the models will be applied to simulate the defined cases with different parameters. The simulations start by specifying the initial values on the free surface, which are determined by using widely-used JONSWAP and Wallops spectra. The JONSWAP is often employed to represent developing sea states[69], which is given in terms of non-dimensional parameters in Table I by

$$S_J(k) = \frac{\alpha_J H_s^2}{2k^3}\exp\left[-\frac{5}{4}\left(\frac{1}{k}\right)^2\right]\gamma^{\exp\left[-\left(\sqrt{k}-1\right)^2/(2\sigma^2)\right]} \tag{12}$$

where H_s is the non-dimensional significant wave height (multiplied by peak wave number), $\alpha_J = 0.0624(1.094 - 0.01915\ln\gamma)/(0.23 + 0.0336\gamma - 0.185(1.9 + \gamma)^{-1})$, γ is the peak enhancement factor, and $\sigma = 0.07$ for $k < 1$ or 0.09 for $k \geq 1$. The bandwidth becomes narrower when γ increases. To represent developed sea states, the Wallops spectrum is often adopted as suggested by Goda[69], which can be expressed by

$$S_W(k) = \frac{\beta H_s^2}{2k^{(m+1)/2}} exp\left[-\frac{m}{4k^2}\right] \tag{13}$$

where $\beta = 0.06238m^{(m-1)/4}/(4^{(m-5)/4}\Gamma[(m-1)/4])[1 + 0.7458(m+2)^{-1.057}]$ and m controls the bandwidth with the spectrum becoming narrower as m increases.

Corresponding to the spectra, the initial linear free surface elevation in the whole domain may be written as

$$\eta'(X, T=0) = \sum_{j=1}^{NJ} a_j\, cos\left(k_j X - \omega_j T + \varphi_j\right)_{T=0} = \sum_{j=1}^{NJ} a_j\, cos\left(k_j X + \varphi_j\right) \tag{14}$$

where $a_j = \sqrt{2S(k_j)\Delta k}$, $S(k)$ can be $S_J(k)$ or $S_W(k)$, and φ_j is randomly distributed in $[0,2\pi)$, k_j is the wave number of the jth component, $\omega_j = \sqrt{k_j}$, NJ is the total number of the components. The limitation by using Eq.(14) (i.e., the random phase technique) was discussed in Tucker, *et al*.[70], who suggested to use the random amplitude approach to give the initial free surface elevation. However, according to Elgar, *et al*.[71], for a sufficiently large number of spectral components (1000 or more), no significant differences were found in the statistics produced by the two techniques. According to this, the total number of components considered is 1024 in the study. More discussions about this will be presented in Section 4.

It is noted that η' by Eq. (14) is merely the free modes. The initial free surface elevation with the bound modes can be constructed by using the technique summarised in APPENDIX C, which was introduced in Wang, *et al*.[50]. The initial free surface conditions may be specified by either considering only the free modes (Eq. 14) or the free modes plus the bound modes. As one of the purposes of this study is to quantify the error of the ENLSE-5F, the simulation of all methods should start with the same initial conditions normally employed by the ENLSE-5F, consisting both free modes and bound modes. In such a way, the errors between their results are mainly attributed to the method itself. If the initial conditions would not be the same, the errors should have included the effects of initial condition, which should not be considered for assessing the accuracy of the methods. Based on these considerations, all simulations for obtaining the results discussed hereafter are carried out by using the initial free surface elevation consisting of both free and bound modes.

A. Computational parameters

To perform the numerical studies, the computational parameters need to be properly selected. This section will discuss how to choose the proper parameters.

There are two parameters in each of the two spectra, which are (H_s, γ) for the JONSWAP and (H_s, m) for

the Wallops spectrum, respectively. In order to quantify the errors of the simplified models, the range of the parameters must be large enough. According to Goda[69], the practical range of γ is within [1, 9] while it is within [5, 25] for m, which will be used in the study here.

In the later sections, the central moment[72] defined by

$$m_c = \int_0^{+\infty} |k-1| \frac{S(k)}{H_s^2} dk \tag{15}$$

will be used. The relationship between m_c and the bandwidth parameters can be established through curve fitting and is given directly here without further details for simplicity, i.e.,

$$m_c = 0.181 \exp(-0.917\gamma^{0.300}) \tag{16}$$

for the JONSWAP spectrum, while

$$m_c = 0.005 \exp(7.807m^{-0.674}) \tag{17}$$

for the Wallops spectrum. The fitted results by the two equations are shown in FIG. 2, where the values denoted by 'target' are those calculated directly by Eq.(15). The maximum error between the target (Eq.15) and fitted results (Eq.16 or Eq.17) are 0.3% and 2.0%, respectively, which is invisible in the figure. From this figure, one can see that the range of m_c is $0.031 \le m_c \le 0.072$ for the JONSWAP spectrum and $0.012 \le m_c \le 0.072$ for the Wallops spectrum with respect to the chosen range of γ and m.

The non-dimensional significant wave height (H_s) actually represents the wave steepness or nonlinearity of the initial free surface elevation as defined in Table I. Note that there are several ways to represent the random wave steepness (ε), e.g., Dysthe, *et al*.[54] used $\varepsilon = \sqrt{2}\sigma$, where $\sigma^2 = \int S(k)dk$. As $H_s = 4\sigma$, one obatins $H_s = 2\sqrt{2}\varepsilon$, which means H_s is directly related to the steepness of the random waves. If it is very small, the waves can be well described by the linear model. Based on this, the lower end of the range of H_s (i.e. its smallest value for the numerical study) is taken as 0.001. The results given in later sections will show that in the ranges of γ and m chosen above, the linear model can very well predict the evolution of waves when $H_s \le 0.001$ (equivalently, $\varepsilon \le 0.0004$).

The question is that what is the largest value of H_s (i.e., the upper end of its range) to be chosen for the numerical studies. It is well known that with the increase of the steepness, the nonlinearity of the waves becomes stronger, the accuracy of the three simplified models decreases and so their errors increase. A model should be considered as unsuitable if its error is larger than a certain value, defined as ER_{up}. In this paper, ER_{up} is chosen to be 20%. The upper end of H_s should be chosen to be the value, corresponding to which the error of all three simplified models is smaller than ER_{up}. According to our numerical tests discussed in later sections, the upper end of H_s can be taken as 0.18 ($\varepsilon \approx 0.064$). Based on the above discussions, the range and specific values of each parameter chosen for numerical studies here are summarised in Table III.

For the numerical studies, the computational domain is set as 128 peak wave lengths, which is more than 20 km if the peak wave period is 10 seconds or more. Based on the tests presented in Wang *et al*.[50] and Wang & Ma[29], the domain is resolved into 8192 points for all the models in Table II. To show the resolution is sufficient, the cases with $H_s = 0.15$ & $m = 5$ for the Wallops spectrum and $H_s = 0.15$ & $\gamma = 1$ for the JONSWAP spectrum ($\varepsilon \approx 0.053$) are studied by using the ESBI with both 8192 and 16384 points. The differences between the results by using two different resolutions are only 2.1% and 2.3% for the Wallops and JONSWAP spectrum, respectively. It means that 8192 points are sufficient for the ESBI. The resolution should also be sufficient for QSBI, ENLSE-5F and linear model as they all involve lower order terms in the computation, which should need a smaller number of computational points than higher order terms to achieve similar results.

B. Effects of duration of simulations

In this subsection, the effects of the duration of simulations will be investigated. The duration should be long enough so that the random waves are fully developed. To quantitatively measure the degree of the wave development, the abnormality indexes[72] are introduced, i.e.,

$$AI_G(T) = \frac{|\partial\eta/\partial X|_{max}}{|\partial\eta/\partial X|_s} \quad , \quad AI_H(T) = \frac{H_{max}}{H_s} \tag{18}$$

where AI_G and AI_H are both functions of T, subscript 'max' represents the maximum value detected within the time range $[0, T]$, $|\partial\eta/\partial X|_s$ is the significant gradient computed by using the initial free surface profile. The two indexes are closely related to the wave statistics and dynamics. For example, AI_H is used for measuring the maximum waves height, which is traditionally adopted for examining the survivability of structures[73]. While AI_G describes the maximum slope of the free surface, on which the wave impact force depends[74].

In order to illustrate how the two indexes evolve with time, the cases with $H_s = 0.15$ & $m = 5$ for the Wallops spectrum and $H_s = 0.15$ & $\gamma = 1$ for the JONSWAP spectrum ($\varepsilon \approx 0.053$) are simulated. The time histories of AI_G and AI_H corresponding to the cases are plotted in FIG. 3. From the figures, one can see that AI_G is not stabilized until $T/T_0 = 300$ while AI_H becomes stable only after $T/T_0 = 600$. Based on this and other tests we carried out, the duration of simulation can be taken as $1000T_0$ to ensure the waves are fully developed. The duration is about 3 hours in real time if the peak period is more than 10 seconds.

FIG. 3 also shows that AI_G and AI_H at the end of simulations obtained by using the ESBI are much higher than these of initial values specified and obtained by using the linear model. In addition, FIG. 3(a) and (c) show that the AI_G obtained by using ESBI is almost double of the initial values and that obtained by using the linear model, while the AI_H from the ESBI is more than 1.5 times larger than others. Compared with the initially specified steepness (i.e., 0.15 in the cases), the obtained maximum slope of the free surface is 0.816 (i.e., 6.8×0.15).

C. Effects of random phases

As discussed above, the initial free surface elevation depends on Eq.(14), which is not deterministic but random as the phase φ_j is random. The question that how this affects the error of each simplified model should be answered priori to further explore the effects of different values of spectrum parameters. Thus some numerical tests are carried out in order to answer this question and the error of each simplified model is measured by

$$Err_{1,2,3} = \frac{\int_0^{L_d} |\eta_{1,2,3} - \eta_0| dX}{\int_0^{L_d} |\eta_0| dX} \tag{19}$$

where $Err_{1\sim3}$ denote the error of the linear model, ENLSE-5F and QSBI, respectively; $\eta_{1\sim3}$ is the corresponding free surface spatial distribution obtained by the three models at the end of the simulation, η_0 that of the ESBI, and L_d is the length of the computational domain. We will mainly focus on two matters: a) one is about the trend of $Err_{1,2,3}$ evolving with time, and b) the other is the statistics of $Err_{1,2,3}$ at the end of the simulation, e.g., average and standard deviation of the error, corresponding to different series of random phases.

For this purpose, the cases with given H_s and γ or m are simulated using all the methods in Table II starting with the same initial condition. The simulations for each set of the computational parameters are repeated 10 times but using a different series of random phases φ_j. $Err_{1,2,3}$ are calculated for each time steps during the simulations. Some examples of $Err_{1,2,3}$ varying with time are shown in FIG. 4, where lines with different colors denote results correspond to different series of random phases. It can be seen that the values of $Err_{1,2,3}$ corresponding to the same parameters of H_s and γ or m are only slightly different for different series of random phases. It implies that even though the initial condition is different due to using different series of random

phases, the evolution of $Err_{1,2,3}$ does not behave significantly differently.

To further show the effects of random phases on $Err_{1,2,3}$, the values of $Err_{1,2,3}$ for several sets of computational parameters obtained at the end of the simulation are extracted. Their average and standard deviation are calculated and presented in Table IV and Table V for the JONSWAP and Wallops spectra, respectively. As can be seen, in the cases where the average error is less than 20%, the maximum standard deviation of the errors is only 1.7%. These data again demonstrate that the values of $Err_{1,2,3}$ are not sensitive to the choice of random series of φ_j.

D. Errors of different simplified models

The errors of different simplified models are now presented and discussed. The method to evaluate the errors has been described above (Eq. (19)), i.e., they are computed by using the wave profiles after simulating the cases with different parameters given in Table III over the duration of $1000T_0$ by 4 different models (the linear model, ENLSE-5F, QSBI and ESBI). For each case, all the four models start with the same initial free surface elevation determined by the method in Appendix C. The errors of the three simplified models (the linear model, ENLSE-5F and QSBI) are then calculated by applying Eq.(19) to the relevant free surface elevations obtained at the end of simulations. The obtained numerical errors in such way are shown by different symbols and indicated by 'calculated' in FIG. 5. It may be noted that the case with the maximum value of H_s is different in different figures. That is because the cases with all the errors are larger than 20% are not plotted in the figures. For an example, in FIG. 5a, the error of the linear model is larger than 20% for the whole range of γ for any value of H_s>0.012 ($\varepsilon > 0.004$) and so the results for the cases with H_s>0.012 are not plotted in the figure. Similarly, the errors for all the other cases with the parameters given in Table III but not plotted in FIG. 5 are all larger than 20%. It may also be noted that the largest values of H_s in all the figures is 0.18, which indicates that all the simplified models have an error larger than 20% if H_s>0.18 ($\varepsilon > 0.064$). This also justifies why we only selected the cases with $H_s \leq 0.18$ (corresponding to ER_{up}= 20%) in Table III. As can be seen from these figures, the errors of each model generally increase with the decrease of γ (or m) and the increase of H_s. With reference to Eq.(16) and (17), it may also be said that the errors increase with the increase of m_c and H_s. In addition, for all the values of γ and m, the errors of the linear model obtained by using the JONSWAP and Wallops spectra are very small, less than 1% for $H_s = 0.001$ ($\varepsilon \approx 0.0004$), which means that the linear model is sufficiently accurate for simulating the cases if the initial significant wave height is less than 0.001.

To mathematically represent the calculated errors in FIG. 5, it is assumed that the calculated errors of the three simplified models can be fitted by

$$Err_1' = a_1 {H_s}^{b_1} {m_c}^{c_1} \tag{20}$$

$$Err_2' = a_2 {H_s}^{b_2} {m_c}^{c_2} \tag{21}$$

$$Err_3' = a_3 {H_s}^{b_3} {m_c}^{c_3} \tag{22}$$

where a_i, b_i and c_i (i = 1, 2 or 3, corresponding to the linear model, ENLSE-5F and QSBI models) are constants to be determined. These constants are determined by optimizing the following target function

$$\mathbb{Y}_i(a_i, b_i, c_i) = \sum_J (Err_i - {Err'}_i)_J^2 \tag{23}$$

where i is taken as 1, 2 or 3, corresponding to the linear model, ENLSE-5F and QSBI; Err_i are these given in FIG. 5 by different symbols, i.e., the calculated values. Since the error larger than 20% may just indicate that a simplified model is not suitable for simulating the random waves as indicated before, only the data corresponding to $Err_i \leq 20\%$ are considered for fitting the numerical results using Eqs.(20), (21) or (22). In order words, the points represented by J in Eq.(23) are only these below the horizontal lines of 20% in FIG. 5.

The optimization is performed by using the toolbox (Optimization-fminsearch) in MATLAB. The details of this toolbox can be found in MATLAB user manual which will not be provided here. After the optimizations are performed, the constants in the fitting formulae corresponding to the JONSWAP spectrum are given by

$$\begin{cases} a_1 = 1.922\times10^4, b_1 = 1.967, c_1 = 0.811 \\ a_2 = 1.207\times10^4, b_2 = 1.944, c_2 = 1.588 \\ a_3 = 3.847\times10^5, b_3 = 4.564, c_3 = 1.726 \end{cases} \tag{24}$$

and these corresponding to the Wallops spectrum are given by

$$\begin{cases} a_1 = 1.280\times10^4, b_1 = 1.971, c_1 = 0.633 \\ a_2 = 4.593\times10^4, b_2 = 1.961, c_2 = 1.942 \\ a_3 = 5.256\times10^4, b_3 = 4.274, c_3 = 1.196 \end{cases} \tag{25}$$

Now, replacing m_c in Eqs. (20) ~ (22) with Eqs. (16) and (17), and substituting $a_{1\sim3}$, $b_{1\sim3}$ and $c_{1\sim3}$ with these in Eqs. (24) and (25), one has

$$Err_1' = 4.805\times10^3 {H_s}^{1.967} \exp(-0.744\gamma^{0.300}) \tag{26}$$

$$Err_2' = 7.997\times10^2 {H_s}^{1.944} \exp(-1.456\gamma^{0.300}) \tag{27}$$

$$Err_3' = 2.013\times10^4 {H_s}^{4.564} \exp(-1.583\gamma^{0.300}) \tag{28}$$

for the JONSWAP spectrum, while

$$Err_1' = 447.4 {H_s}^{1.971} \exp(4.942 m^{-0.674}) \tag{29}$$

$$Err_2' = 1.561 {H_s}^{1.961} \exp(15.161 m^{-0.674}) \tag{30}$$

$$Err_3' = 93.03 {H_s}^{4.274} \exp(9.337 m^{-0.674}) \tag{31}$$

for the Wallops spectrum.

The curves of Err'_i are plotted in FIG. 5, denoted by 'fitted'. One can see that there is excellent consistency between the calculated and fitted results for all the cases with $Err_{1\sim3} \leq 20\%$. The maximum differences between the calculated and fitted results obtained by using the JONSWAP spectrum and Wallops spectrum are only 2.1% occurring at the point for $H_s = 0.11$ ($\varepsilon \approx 0.039$) and $\gamma = 1$ in FIG. 5c and 1.9% occurring at the point for $H_s = 0.15$ ($\varepsilon \approx 0.053$) and $m = 25$ in FIG. 5f, respectively.

It is noted that as Eqs. (26)~(31) are obtained by using the cases with the parameters listed in Table III, they may be perceived to be only applicable within the range $0.001 \leq H_s \leq 0.18$ ($0.0004 \leq \varepsilon \leq 0.064$), $5 \leq m \leq 25$ for Wallops spectrum and $1 \leq \gamma \leq 9$ for JONSWAP spectrum. However, as aforementioned, the linear model can provide accurate results while $H_s < 0.001$ and the errors are larger than 20% if $H_s > 0.18$. In addition, when $Err_{1\sim3} > 20\%$, it just indicates that the corresponding model cannot give acceptable results for modelling the random sea in deep water. Taking all the facts into account, one may know from the results presented in this section that (1) when $H_s < 0.001$, the linear model can be used without significant error; (2) when $H_s > 0.18$, none of the three simplified models should be employed; (3) when $0.001 \leq H_s \leq 0.18$, one can estimate the errors of the three simplified models: if the error of a model is less than 20%, this error needs to be accepted if using this model; if the error is larger than 20%, this model may not be employed.

In addition, Eqs. (26)~(31) can be reformulated to find the maximum significant wave height, within which the simplified models can be adopted while maintaining acceptable accuracy. To do so, one should specify a tolerance (Tol) and ensure that the condition $Err' \leq Tol$ is met for the selected model. Then Eqs. (26)~(31) are replaced by the expressions with respect to the dimensionless significant wave height, i.e., for the JONSWAP spectrum

$$Hs_1 = 0.013\exp(0.378\gamma^{0.3})\,Tol^{0.508} \quad (32)$$

$$Hs_2 = 0.032\exp(0.749\gamma^{0.3})\,Tol^{0.514} \quad (33)$$

$$Hs_3 = 0.114\exp(0.347\gamma^{0.3})\,Tol^{0.219} \quad (34)$$

and for the Wallops spectrum

$$Hs_1 = 0.045\exp(-2.507m^{-0.674})\,Tol^{0.507} \quad (35)$$

$$Hs_2 = 0.797\exp(-7.731m^{-0.674})\,Tol^{0.510} \quad (36)$$

$$Hs_3 = 0.346\exp(-2.185m^{-0.674})\,Tol^{0.234} \quad (37)$$

where Hs_i (i=1,2 or 3) is the maximum significant wave height for the linear model, ENLSE-5F and QSBI to be employed, respectively.

More discussions about how to use Eqs. (26)~(31) and Eqs. (32)~(37) will be given in the following sections.

4 DISCUSSIONS

This section will discuss several points relevant to Eqs. (26)~(31) and Eqs. (32)~(37), including their possible applications to evaluating the simplified models that are employed to study the random wave dynamics or statistics.

A. Comparisons with the criterion of Dysthe, *et al.*'s[52]

Dysthe, *et al.*[52] had pointed out that the CNLSE and MNLSE can be reliably used on a temporal scale up to $2\varepsilon^{-2}$ and $10\varepsilon^{-2}$, respectively, for simulating narrow bandwidth waves (initial conditions determined by the Gaussian Spectrum). Based on them, for simulations of 1000 peak periods ($T_0 = 2\pi$), the CNLSE and MNLSE can be used with the significant wave height ($H_s = 2\sqrt{2}\varepsilon$) up to about 0.05 and 0.11 ($\varepsilon \approx 0.018$ and 0.039), respectively. The criterion of Dysthe, *et al.*[52] is compared with these we suggested, i.e., Eqs. (32)~(37) for $Tol = 10\%$ in FIG. 8. The grey thicker dashed line denotes the up-limit of the MNLSE and the grey thinner dashed line represents that of the CNLSE based on the suitable temporal scale given by Dysthe, *et al.*[52]. It can be observed in both FIG. 8(a) and (b) that the up-limit of the MNLSE is significantly higher than these given for the ENLSE-5F model in this study, in particular for the cases corresponding to the JONSWAP spectrum. The former is only close to the latter when the Wallops spectrum with very narrow bandwidth (m>20) is used. It means that if the suggestion of Dysthe, *et al.*[52] for MNLSE is followed, the results may have the error much larger than 10%. The same argument applies to the CNLSE employed for the JONSWAP spectrum as shown in FIG. 8(a). Furthermore, if the initial conditions of the CNLSE are specified by the Wallops spectrum, the up-limit of CNLSE model indicated by $2\varepsilon^{-2}$ is much different from what we give here even for the waves with a very narrow bandwidth. This implies that if the suggestion of Dysthe, *et al.*[52] is followed, one would not obtain the results that bear the error of less than 10%.

B. Error prediction

Eqs. (26)~(31) can be employed for predicting the error of the simplified models. To illustrate their effectiveness, extra numerical tests are carried out for the cases with parameters listed in Table VI and Table VII, which are in the range of the parameters in Table III but different from those used for obtaining the results in FIG. 5. In the tables, the values of $Err_{1\sim3}$ are obtained in the same way as for FIG. 5, while the values of $Err'_{1\sim3}$ are predicted by Eqs. (26)~(31) for the corresponding parameters. These errors represented by '-' in the tables means that their values are larger than 20%. It is found that although the choices of the parameters differ from these in FIG. 5, Eqs. (26)~(31) can still satisfactorily give quite accurate prediction of the errors as long as $Err_{1\sim3} < 20\%$. The maximum deviation between the calculated and predicted errors in these cases is about 1.4%, which is below the maxima indicated in Section 3.

To show the level of correlation between the error given in Eqs. (26)~(31) and wave elevations, some wave profiles at the end of the simulation corresponding to different level of errors are displayed in FIG. 6. It can be seen that as long as the predicted error is small, the differences between the elevations calculated by the simplified models and these by the ESBI are almost invisible. We have also examined the corresponding velocity and velocity potential, and found that the errors of the velocity and velocity potential are in the same magnitude as those of the wave elevations if $Err_{1\sim3} < 20\%$ (results are not presented here for shortening the length of the paper).

As aforementioned, some studies employ the random amplitude approach to convert the spectrum to the free surface elevation[70,75]. As discussed in the former section, the results of the random amplitude approach are approximately the same with these of the random phase approach when the number of wave component is large[71]. To show that Eqs. (26)~(31) are also correlated with the error in the cases where the random amplitude technique is adopted for generating the initial free surface condition, we carry out the numerical tests on the cases with the parameters in Table VI and Table VII by using the random amplitude approach. The calculated and predicted errors are shown in Table VIII and Table IX. It is found the maximum difference between the calculated errors obtained by using the random amplitude approach and these predicted by Eqs. (26)~(31) is only 1.6%. The spatial distribution of the free surface for some cases are also presented in FIG. 7. These figures show that the results are very similar to FIG. 6. All the facts demonstrate that Eqs. (26)~(31) can be used to predict the errors in the cases where random amplitude approach would be used for generating the initial free surface condition.

C. Suitability of simplified models

In order to study random waves on large-spatial and long-temporal scale in deep water efficiently and accurately, one should firstly determine suitable model among the linear model, ENLSE-5F, QSBI and ESBI. In this section, graphs showing the regions suitable for different models will be presented, which may help researchers to select a model.

When selecting the model, the acceptable error should be specified, such as no more than 5% as indicated by Wang, *et al*.[50]. Based on Eqs. (32)~(37), the graphs of the maximum significant wave height Hs_i (i=1,2 or 3) suitable for different models are plotted in FIG. 9 with respect to tolerant error $Tol = 5\%$. The graphs illustrate the regions in which different models are suitable. For example, the ENLSE-5F is suitable for simulating all the cases underneath the dot-dashed lines. It is illustrated that the maximum significant wave height for a specific model to be applied increases when the bandwidth becomes smaller (γ or m becomes larger) for both the spectra. The reason is that the terms ignored in the simplified model involves the bandwidth parameter. Such terms become more and more important and dominating when bandwidth increases, so that they become less accurate. As a consequence, in order to maintain the same level of accuracy, the maximum significant wave height that the simplified model could be applied becomes smaller as the bandwidth increases, or becomes larger as the bandwidth decreases (γ or m increases).

According to these aforementioned, it is suggested that the following conditions

$$H_s \le Hs_1\text{: Linear model} \tag{38}$$

$$Hs_1 < H_s \le Hs_2\text{: ENLSE-5F} \tag{39}$$

$$Hs_2 < H_s \le Hs_3\text{: QSBI} \tag{40}$$

$$H_s > Hs_3\text{: Fully nonlinear model} \tag{41}$$

can be used as the criterion for selecting a model to simulate random seas on large-spatial and long-temporal scales in deep water. That is to say, if the condition of Eq. (38) is met, the linear model is selected; if Eq. (39) is satisfied, the ENLSE-5F is employed; while QSBI should be adopted for the condition of Eq. (40) to be satisfied; otherwise, the fully nonlinear model should be employed.

It is noted that for the very strong nonlinear cases the breaking wave will occur and so fully nonlinear model ESBI will not be suitable. The up-limit of the fully nonlinear model, beyond which breaking wave occurs, were discussed by Melville[76] and Ochi & Tsai[77] for uniform wave cases. Identifying the up-limit of the ESBI is beyond the scope of this study, as we mainly focus on identifying the boundaries of the simplified models.

5 CONCLUDING REMARKS

This paper has presented the formulas for quantitatively estimating the errors of the Enhanced Nonlinear Schrödinger Equation based on Fourier transform (ENLSE-5F) and Quasi Spectral Boundary Integral (QSBI) method when they are applied for simulating nonlinear random waves in deep sea on large-spatial and long-temporal scales in a phase-resolved manner. The two groups of formulas are given, one for the initial conditions specified by the JONSWAP spectrum and the other by the Wallops spectrum. The suggested formulas can give good predictions on the errors of the simplified models as long as the errors are less than 20% within the range of bandwidth in $1 \le \gamma \le 9$ or $5 \le m \le 25$ and the significant wave height in $Hs \le 0.18$ ($\varepsilon \le 0.064$). The ranges of bandwidth parameters are considered to cover the most cases met in real sea states according to the literature available. If the error is larger than 20% estimated by the formulas and/or $Hs > 0.18$ ($\varepsilon > 0.064$), it just means that the simplified models may not give acceptable results and so may not be employed. Although the formulas are obtained by using initial condition based on random phase approach, they also work for those cases based on random amplitude approach according to the numerical tests.

Based on the formulas, the suitable regions for the simplified models are plotted in terms of bandwidth parameters (γ for the JONSWAP spectrum and m for the Wallops spectrum) and significant wave heights (i.e., peak wave number times significant wave height). The dimensionless maximum significant wave height up to which the simplified model could be applied becomes smaller as the bandwidth increases, or becomes larger as bandwidth decreases (γ or m increases), which are quite different from the qualitative indication available in literature.

This paper provides useful information for evaluating the simplified wave models that are employed for studying random wave dynamics, e.g., how reliable are the results obtained after using the simplified models, or which model should be selected in order to obtain acceptable results before carrying out the simulations. However, it should be pointed out that although the formulas proposed in this paper are based on the cases of unidirectional waves, they also give an indication of the errors for the simplified models to be applied for simulating spreading seas. However, further studies on their errors in simulating spreading seas will be carried out in the future.

ACKNOWLEDGMENTS

This work was supported by the EPSRC, UK (EP/N008863/1, EP/L01467X/1 and EP/N006569/1).

APPENDIX A: HARMONIC COEFFICIENTS

In order to estimate the free surface and velocity potential, each harmonic coefficient is given in terms of A by Wang, *et al*.[50], which follow as

$$A_2 = \frac{1}{2}A^2 - \frac{i}{2}A\frac{\partial A}{\partial X} + \frac{3}{8}A\frac{\partial^2 A}{\partial X^2} \tag{A. 1}$$

$$A_3 = \frac{3}{8}A^3 \tag{A. 2}$$

$$B = F^{-1}\left\{\frac{-i}{\omega}F\left\{A + \frac{3}{8}|A|^2 A\right\}\right\} \tag{A. 3}$$

$$B_2 = B_3 = 0 \tag{A. 4}$$

$$\bar{\phi} = F^{-1}\left\{sgn(\kappa)\frac{i}{2}F\{|A|^2\}\right\} \tag{A. 5}$$

$$\bar{\eta} = F^{-1}\{-isgn(\kappa)F\{real(A^* A_T)\}\} - \frac{1}{16}\frac{\partial^2 |A|^2}{\partial X^2} \tag{A. 6}$$

APPENDIX B: FORMULATIONS FOR VERTICAL VELOCITY

The formulations for estimating the convolution and integration parts in the vertical velocity V have been proposed by Grue[28] and Wang & Ma[29], which are also presented below

$$V_1 = F^{-1}\left\{KF\{\tilde{\phi}\}\right\} \tag{B. 1}$$

$$V_2 = -F^{-1}\{KF\{\eta V_1\}\} - \nabla\cdot(\eta\nabla\tilde{\phi}) \tag{B. 2}$$

$$V_3 = F^{-1}\left\{\frac{K}{2\pi}F\left\{\int_{S_0}\tilde{\phi}'\left[1 - \frac{1}{(1+D^2)^{3/2}}\right]\frac{(\eta'-\eta)-\boldsymbol{R}\cdot\nabla'\eta'}{R^3}d\boldsymbol{X}'\right\}\right\} \tag{B. 3}$$

$$\begin{aligned} V_4 = &-\frac{K}{2}\left[KF\{\eta^2 V\} - 2F\left\{\eta F^{-1}\{KF\{\eta V\}\}\right\} + F\left\{\eta^2 F^{-1}\{KF\{V\}\}\right\}\right] \\ &+ \frac{K}{2\pi}F\left\{\int\frac{V'}{R}\left(1 - \frac{1}{\sqrt{1+D^2}} - \frac{1}{2}D^2\right)d\boldsymbol{X}'\right\} \end{aligned} \tag{B. 4}$$

$$\begin{aligned} F\left\{V_3^{(1)}\right\} = &-\frac{K}{6}\left[Ki\boldsymbol{K}\cdot F\{\eta^3\nabla\tilde{\phi}\} - 3F\left\{\eta F^{-1}\left\{Ki\boldsymbol{K}\cdot F\{\eta^2\nabla\tilde{\phi}\}\right\}\right\}\right. \\ &\left. + 3F\left\{\eta^2 F^{-1}\left\{Ki\boldsymbol{K}\cdot F\{\eta\nabla\tilde{\phi}\}\right\}\right\} + F\left\{\eta^3 F^{-1}\left\{K^3 F\{\tilde{\phi}\}\right\}\right\}\right] \end{aligned} \tag{B. 5}$$

$$\begin{aligned} F\left\{V_3^{(2)}\right\} = &-\frac{K}{120}\left[i\boldsymbol{K}K^3\cdot F\{\eta^5\nabla\tilde{\phi}\} - 5F\left\{\eta F^{-1}\left\{i\boldsymbol{K}K^3\cdot F\{\eta^4\nabla\tilde{\phi}\}\right\}\right\}\right. \\ &+ 10F\left\{\eta^2 F^{-1}\left\{i\boldsymbol{K}K^3\cdot F\{\eta^3\nabla\tilde{\phi}\}\right\}\right\} \\ &- 10F\left\{\eta^3 F^{-1}\left\{i\boldsymbol{K}K^3\cdot F\{\eta^2\nabla\tilde{\phi}\}\right\}\right\} \\ &\left. + 5F\left\{\eta^4 F^{-1}\left\{i\boldsymbol{K}K^3\cdot F\{\eta\nabla\tilde{\phi}\}\right\}\right\} + F\left\{\eta^5 F^{-1}\left\{K^5 F\{\tilde{\phi}\}\right\}\right\}\right] \end{aligned} \tag{B. 6}$$

$$\begin{aligned} F\{V_{3,I}\} = &\frac{K}{2\pi}F\left\{\frac{35}{16}\int\tilde{\phi}'\nabla'\cdot\left[(\eta'-\eta)\nabla'\frac{1}{R}\right]D^6 d\boldsymbol{X}'\right. \\ &+ \int\tilde{\phi}'\left[1 - (1+D^2)^{-3/2} - \frac{3}{2}D^2 + \frac{15}{8}D^4 - \frac{35}{16}D^6\right]\nabla' \\ &\left.\cdot\left[(\eta'-\eta)\nabla'\frac{1}{R}\right]d\boldsymbol{X}'\right\} \end{aligned} \tag{B. 7}$$

$$F\left\{V_4^{(2)}\right\} = -\frac{K}{24}\Big[K^3F\{V\eta^4\} - 4F\left\{\eta F^{-1}\left\{K^3F\{V\eta^3\}\right\}\right\} + 6F\left\{\eta^2F^{-1}\left\{K^3F\{V\eta^2\}\right\}\right\} - 4F\left\{\eta^3F^{-1}\left\{K^3F\{V\eta\}\right\}\right\} + F\left\{\eta^4F^{-1}\left\{K^3F\{V\}\right\}\right\}\Big] \tag{B. 8}$$

$$F\left\{V_4^{(3)}\right\} = \frac{-K}{720}\Big[K^5F\{V\eta^6\} - 6F\left\{\eta F^{-1}\left\{K^5F\{V\eta^5\}\right\}\right\} + 15F\left\{\eta^2F^{-1}\left\{K^5F\{V\eta^4\}\right\}\right\} - 20F\left\{\eta^3F^{-1}\left\{K^5F\{V\eta^3\}\right\}\right\} + 15F\left\{\eta^4F^{-1}\left\{K^5F\{V\eta^2\}\right\}\right\} - 6F\left\{\eta^5F^{-1}\left\{K^5F\{V\eta\}\right\}\right\} + F\left\{\eta^6F^{-1}\left\{K^5F\{V\}\right\}\right\}\Big] \tag{B. 9}$$

$$F\{V_{4,I}\} = \frac{K}{2\pi}F\left\{\int \frac{V'}{R}\left(1 - \frac{1}{\sqrt{1+D^2}} - \frac{1}{2}D^2 + \frac{3}{8}D^4 - \frac{5}{16}D^6\right)d\boldsymbol{X}'\right\} \tag{B. 10}$$

APPENDIX C: CONSTRUCTION OF ENVELOPE FROM FREE SURFACE ELEVATION

According to Eq. (9), the free surface elevation can be rewritten as

$$\eta = \bar{\eta} + \eta_1 + \eta_2 + \eta_3 \tag{C. 1}$$

where

$$\eta_1 = \frac{1}{2}\left(Ae^{i\theta} + c.c.\right), \quad \eta_2 = \frac{1}{2}\left(A_2e^{2i\theta} + c.c.\right), \quad \eta_3 = \frac{1}{2}\left(A_3e^{3i\theta} + c.c.\right). \tag{C. 2}$$

Introducing Hilbert transform $\mathcal{H}\{\eta_1(X)\} = \frac{1}{\pi}\int_{-\infty}^{\infty}\frac{\eta_1(X')}{X'-X}dX'$ to η_1 and rearranging it gives

$$A = e^{-i(X-T)}(\eta_1 - i\mathcal{H}\{\eta_1\}). \tag{C. 3}$$

Note that $\mathcal{H}\{\eta_1\} = F^{-1}\{i\ sgn(\kappa)F\{\eta_1\}\}$, then the equation above becomes

$$A = e^{-i(X-T)}\left(\eta_1 + F^{-1}\{sgn(\kappa)F\{\eta_1\}\}\right). \tag{C. 4}$$

Initially, η_1 is equals to η' obtained by using Eq.(14). By using Eq.(A1)~(A6) and Eq.(9) and (10) and specifying *T=0*, the initial free surface and velocity potential can be reconstructed, which will be used as the initial condition for the ESBI and QSBI, while the envelope A by Eq.(C.4) is used as the initial condition for the ENLSE-5F.

REFERENCES

[1]Xiao W, Liu Y, Wu G, Yue DKP. "Rogue wave occurrence and dynamics by direct simulations of nonlinear wave-field evolution". J. Fluid Mech. 720, p. 357-392(2013).

[2]Hasselmann K. "On the non-linear energy transfer in a gravity-wave spectrum. Part I: General theory". J. Fluid Mech. 12, p. 481-500(1962).

[3]Phillips OM. "Wave interactions - the evolution of an idea". Journal of Fluid Mechanics. 106, p. 215-227(1981).

[4]Komen GJ, Cavaleri L, Donelan M, Hasselmann K, Hasselmann S, Janssen PAEM. "Dynamics and modeling of ocean waves". New York: Cambridge University Press(1996).

[5]Wu G. “Direct Simulation and Deterministic Prediction of Large-scale Nonlinear Ocean Wave-field (PhD Thesis)”. Massachusetts, USA: Massachusetts Institute of Technology(2004).
[6]Clauss GF, Schmittner CE, Stuck R. “Numerical wave tank - simulation of extreme waves for the investigation of structural responses”. In 24th International Conference on Offshore Mechanics and Arctic Engineering. Halkidiki, Greece(2005).
[7]Grilli ST, Harris J, Greene N. “Modeling of wave-induced sediment transport around obstacles”. In Proc. 31st Intl. Coastal Engng. Conf. Hamburg, Germany, pp.1638-1650(2008).
[8]Haussling HJ, Van Eseltine RT. “Finite-Difference Methods for Transient Potential Flows with Free Surfaces”. In Proceedings of the 1st International Conference on Numerical Ship Hydrohynamics. Gaithersburg, Mariland(1975).
[9]Bingham HB, Zhang H. “On the accuracy of finite-difference solutions for nonlinear water waves”. Journal of Engineering Mathematics. 58, p. 211-228(2007).
[10]Engsig-Karup AP, Bingham HB, Lindberg O. “An efficient flexible-order model for 3D nonlinear water waves”. Journal of Computational Physics. 228(6): p. 2100-2118(2009).
[11]Longuet-Higgins MS, Cokelet ED. “The deformation of steep surface waves on water”. I. A numerical method of computation. Pro. R. Soc. Lond. A. 350, p. 1-26(1976).
[12]Grilli ST, Guyenne P, Dias F. “A fully non-linear model for three-dimensional overturning waves over an arbitrary bottom”. International Journal for Numerical Methods in Fluids. 35, p. 829-867(2001).
[13]Wu GX, Eatock-Taylor R. “Finite element analysis of two dimensional non-linear transient water waves”. Appl. Ocean Res. 16, p. 363-372(1994).
[14]Ma QW. “Numerical simulation of nonliear interaction between structures and steep waves (PhD Thesis)”. London: Department of Mechanical Enginieering, University College London, UK(1998).
[15]Yan S. “Numerical simulation on nonlinear response of moored floating structures to steep waves (PhD thesis)”. London, UK: School of Engineering and Mathematical Sciences, City University London(2006).
[16]Ma QW, Yan S. “Quasi ALE finite element method for nonlinear water waves”. Journal of Computational Physics. 212, p. 52-72(2006).
[17]Baldock TE, Swan C. “Numerical calculations of large transient water waves”. Applied Ocean Research. 16(2), p. 101-112(1994).
[18]Johannessen TB, Swan C. “Nonlinear transient water waves—part I. A numerical method of computation with comparisons to 2-D laboratory data”. Applied Ocean Research. 19(5), p. 293-308(1997).
[19]Chalikov D, Babanin AV. “Three-Dimensional Periodic Fully Nonlinear Potential Waves”. In ASME 2013 32nd International Conference on Ocean, Offshore and Arctic Engineering. Nantes, France(2013).
[20]Craig W, Sulem C. “Numerical simulation of gravity waves”. J. Comput. Phys. 108, p. 73-83(1993).
[21]Nicholls DP. “Traveling Water Waves: Spectral Continuation Methods with Parallel Implementation”. Journal of Computational Physics. 143(1), p. 224-240(1998).
[22]Bateman WJD, Swan C, Taylor PH. “On the efficient numerical simulation of directionally spread surface water waves”. J. Comput. Phys. 174, p. 277-305(2001).
[23]Kim JW, Ertekin RC. “A numerical study of nonlinear wave interaction in regular and irregular seas: irrotational Green–Naghdi model. Marine structures”. 13(4), p. 331-347(2000).
[24]West BJ, Brueckner KA, Janda RS, Milder DM, Milton RL. “A new numerical method for surface hydrodynamics”. Journal of Geophysical Research: Oceans. 92(C11), p. 11803-11824(1987).

[25]Dommermuth DG, Yue DKP. “A high-order spectral method for the study of nonlinear gravity waves”. J. Fluid Mech. 184, p. 267-288(1987).
[26]Clamond D, Grue J. “A fast method for fully nonlinear water-wave computations”. J. Fluid Mech. 447, p. 337-355(2001).
[27]Fructus D, Kharif C, Francius M, Kristiansen Ø, Clamond D, Grue J. “Dynamics of crescent water wave patterns”. Journal of Fluid Mechanics. 537, p. 155-186(2005).
[28]Grue J. “Computation formulas by FFT of the nonlinear orbital velocity in three-dimensional surface wave fields”. J. Eng. Math. 67, p. 55-69(2010).
[29]Wang J, Ma QW. “Numerical techniques on improving computational efficiency of Spectral Boundary Integral Method. International Journal for Numerical Methods in Engineering”. 102(10), p. 1638-1669(2015).
[30]Ducrozet G, Bonnefoy E, Touze DL, Ferrant P. “3-D HOS simulation of extreme waves in open seas”. Nat. Hazards Earth Syst. Sci. 7, p. 109-122(2007).
[31]Kriebel DL. “Nonlinear wave interaction with a vertical circular cylinder. Part I: Diffraction theory”. Ocean Engineering. 17(4), p. 345-377(1990).
[32]Kriebel DL. “Nonlinear wave interaction with a vertical circular cylinder. Part II: Wave run-up. Ocean Engineering”. 19(1), p. 75-99(1992).
[33]Boussinesq J. “Théorie de l'intumescence liquide, applelée onde solitaire ou de translation, se propageant dans un canal rectangulaire”. Comptes Rendus de l'Academie des Sciences. 72, p. 755-759(1871).
[34]Korteweg DJ, de Vries G. “On the change of form of long waves advancing in a rectangular cannal, and on a new type of long stationary waves”. Phil. Mag. 39, p. 422-443(1895).
[35]Wei G, Kirby JT, Grilli ST, Subramanya R. “A fully nonlinear Boussinesq model for surface waves. Part 1. Highly nonlinear unsteady waves”. J. Fluid Mech. 294, p. 71-92(1995).
[36]Madsen PA, Bingham HB, Liu H. “A new Boussinesq method for fully nonlinear waves from shallow to deep water”. Journal of Fluid Mechanics. 462, p. 1-30(2002).
[37]Lynett PJ, Liu PLF. “Linear analysis of the multi-layer model”. Coastal Engineering. 51, p. 439-454(2004).
[38]Grue J, Pelinovsky EN, Fructus D, Talipova T, Kharif C. “Formation of undular bores and solitary waves in the Strait of Malacca caused by the 26 December 2004 Indian Ocean tsunami”. Journal of Geophysical Research: Oceans. 113(C5), p. 1-14(2008).
[39]Wang J, Ma QW. “Numerical Investigation on Limitation of Boussinesq Equation for Generating Focusing Waves”. Procedia Engineering. 126, p. 597-601(2015).
[40]Zakharov VE. “Stability of periodic waves of finite amplitude on the surface of a deep fluid”. Sov. Phys. J. Appl. Mech. Tech. Phys. 9, p. 86-94(1968).
[41]Annenkov SY, Shrira VI. “Numerical modelling of water-wave evolution based on the Zakharov equation”. Journal of Fluid Mechanics. 449, p. 341-371(2001).
[42]Zakharov VE, Dyachenko AI, Vasilyev OA. “New method for numerical simulation of a nonstationary potential flow of incompressible fluid with a free surface”. European Journal of Mechanics-B/Fluids. 21(3), p. 283-291(2002).
[43]Benney DJ, Roskes GJ. “Wave instabilities”. Studies in Applied Mathematics. 48, p. 377-385(1969).
[44]Davey A, Stewartson K. “On three-dimensional packets of surface waves”. Proc. R. Soc. Lond. A. 388, p. 101-110(1974).
[45]Dysthe KB. “Note on a modification to the nonlinear Schrödinger equation for application to deep water waves”. Proc. R. Soc. Lond. A. 369, p. 105-114(1979).

[46]Stiassnie M. “Note on the modified nonlinear Schrödinger equation for deep water waves”. Wave Motion. 6, p. 431-433(1984).
[47]Trulsen K, Dysthe KB. “A modified nonlinear Schrödinger equation for broader bandwidth gravity waves on deep water”. Wave motion. 24, p. 281-298(1996).
[48]Trulsen K, Kliakhandler I, Dysthe KB, Velarde MG. “On weakly nonlinear modulation of waves on deep water”. Physics of Fluids. 12 (10), p. 2432-2437(2000).
[49]Debsarma S, Das KP. “A higher-order nonlinear evolution equation for broader bandwidth gravity waves in deep water”. Physics of Fluids. 14(104101), p. 1-8(2005).
[50]Wang J, Ma QW, Yan S. “A hybrid model for simulating rogue waves in random seas on a large time and space scale”. Journal of Computational Physics. 313, p. 279-309(2016).
[51]Onorato M, Osborne AR, Serio M, Bertone S. “Freak waves in random oceanic sea states”. Physical review letters. 86(25), p. 5831-5834(2001).
[52]Dysthe KB, Trulsen K, Krogstad HE, Socquet-Juglard H. “Evolution of a narrow-band spectrum of random surface gravity waves”. Journal of Fluid Mechanics. 478, p. 1-10(2003).
[53]Onorato M, Osbourne AR, Serio MAA, Resio D, Pushharev A, Zakharov VE, & Brandini, C. “Freely decaying weak turbulence for sea surface gravity waves”. Physical review letters. 89(14), p. 144501(2002).
[54]Dysthe K, Socquet-Juglard H, Trulsen K, Krogstad HE, Liu J. “’Freak’ waves and large-scale simulations of surface gravity waves”. In Proc. 14th ‘Aha Huliko‘ a Hawaiian Winter Workshop, Honolulu, Hawaii(2005).
[55]Socquet-Juglard H, Dysthe K, Trulsen K, Krogstad HE, Liu J. “Probability distributions of surface gravity waves during spectral changes”. Journal of Fluid Mechanics. 542, p. 195-216(2005).
[56]Shemer L, Sergeeva A, Sunyaev A. “Applicability of envelope model equations for simulation of narrow-spectrum unidirectional random wave field evolution: Experimental validation”. Physics of Fluids. 22, p. 016601 1-9(2010).
[57]Onorato M, Proment D, Toffoli A. “Triggering rogue waves in opposing currents”. Phys. Rev. Lett. 107(18), p. 184502-184507(2011).
[58]Ruban VP. “On the nonlinear Schrödinger equation for waves on a nonuniform current”. JETP letters. 95(9), p. 486-491(2012).
[59]Zeng H, Trulsen K. “Evolution of skewness and kurtosis of weakly nonlinear unidirectional waves over a sloping bottom”. Natural Hazards and Earth System Sciences. 12(3), p. 631-638(2012).
[60]Sergeeva A, Slunyaev A, Pelivosky E, Talipova T, Doong DJ. “Numerical modeling of rogue waves in coastal waters”. Natural Hazards and Earth System Sciences. 14(4), p. 861-870(2014).
[61]Taklo TMA, Trulsen K, Gramstad O, Krogstad HE, Jensen A. “Measurement of the dispersion relation for random surface gravity waves”. Journal of Fluid Mechanics. 766, p. 326-336(2015).
[62]Adcock TAA, Taylor PH, Draper S. “Nonlinear dynamics of wave-groups in random seas: unexpected walls of water in the open ocean”. Proceedings of the Royal Society A: Mathematical, Physical and Engineering Sciences. 471, p. 20150660(2015).
[63]Simanesew A, Krogstad HE, Trulsen K, Borge JCN. “Development of frequency-dependent ocean wave directional distributions”. Applied Ocean Research. 59, p. 304-312(2016).
[64]Zhang HD, Soares CG, Onorato M, Toffoli A. “Modelling of the temporal and spatial evolutions of weakly nonlinear random directional waves with the modified nonlinear Schrödinger equations”. Applied Ocean Research. 55, p. 130-140(2016).

[65]Clamond D, Francius M, Grue J, Kharif C. “Long time interaction of envelope solitons and freak wave formations”. European Journal of Mechanics B/Fluids. 25, p. 536-553(2006).
[66]Wang J. “A hybrid model for large scale simulation of unsteady nonlinear waves (PhD Thesis)”. London, UK: City University London(2016).
[67]Xiao W. “Study of directional ocean wavefield evolution and rogue wave occurrence using large-scale phase-resolved nonlinear simulations (PhD thesis)”. Cambridge, United States: Massachusetts Institute of Technology(2013).
[68]Fructus D, Clamond D, Grue J, Kristiansen O. “An efficient model for three-dimensional surface wave simulations Part I: Free space problems”. Journal of Computational Physics. 205, p. 665-685(2005).
[69]Goda Y. “A comparative review on the functional forms of directional wave spectrum”. Coastal Engineering Journal. 41(1), p. 1-20(1999).
[70]Tucker MJ, Challenor PG, Carter DJT. “Numerical simulation of a random sea: a common error and its effect upon wave group statistics”. Applied ocean research. 6(2), p. 118-122(1984).
[71]Elgar S, Guza RT, Seymour RJ. “Wave group statistics from numerical simulations of a random sea”. Applied ocean research. 7(2), p. 93-96(1985).
[72]Kharif C, Pelinovsky E, Slunyaev A. “Rogue Waves in the Ocean”. Berlin Heidelberg: Springer-Verlag(2009).
[73]DNV. “Recommended Practice Self-elevating Units”. 104th ed. Norway: DET NORSKE VERITAS(2011).
[74]Wienke J, Oumeraci H. “Breaking wave impact force on a vertical and inclined slender pile—theoretical and large-scale model investigations”. Coastal Engineering. 52(5), p. 435-462(2005).
[75]Taylor PH, Jonathan P, Harland LA. “Time domain simulation of jack-up dynamics with the extremes of a Gaussian process”. Journal of vibration and acoustics. 119(4), p. 624-628(1997).
[76]Melville WK. “The instability and breaking of deep-water waves”. Journal of Fluid Mechanics. 115, p. 165-185(1982).
[77]Ochi MK, Tsai CH. “Prediction of occurrence of breaking waves in deep water”. Journal of physical oceanography. 13(11), p. 2008-2019(1983).
[78]Zakharov VE, Dyachenko AI. “About shape of giant breather”. European Journal of Mechanics-B/Fluids, 29(2), p.127-131(2010).
[79]Craig W, Guyenne P, Sulem C. “Hamiltonian higher-order nonlinear Schrödinger equations for broader-banded waves on deep water”. European Journal of Mechanics-B/Fluids, 32, p. 22-31(2012).
[80]Gramstad O, Trulsen K. “Hamiltonian form of the modified nonlinear Schrödinger equation for gravity waves on arbitrary depth”. Journal of Fluid Mechanics, 670, p.404-426(2011).
[81]Craig W, Guyenne P, Sulem, C. “A Hamiltonian approach to nonlinear modulation of surface water waves”. Wave Motion, 47(8), p.552-563(2010).

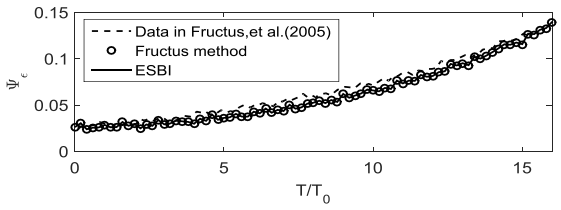

FIG. 1. Evolution of perturbation components of $\boldsymbol{K} = (3/2, 4/3)$

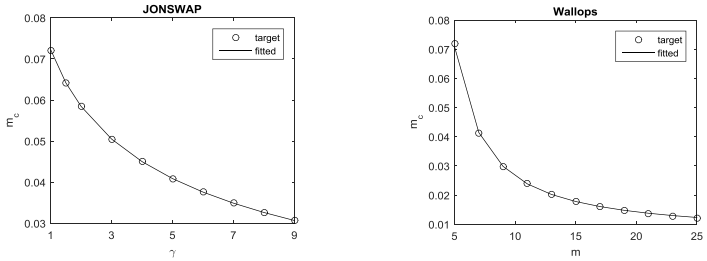

(a) (b)

FIG. 2. Fitting results of (a) $m_c \sim \gamma$ and (b) $m_c \sim m$

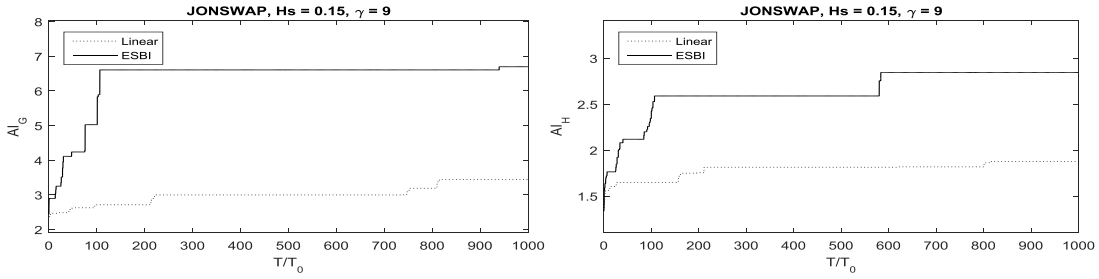

(a) (b)

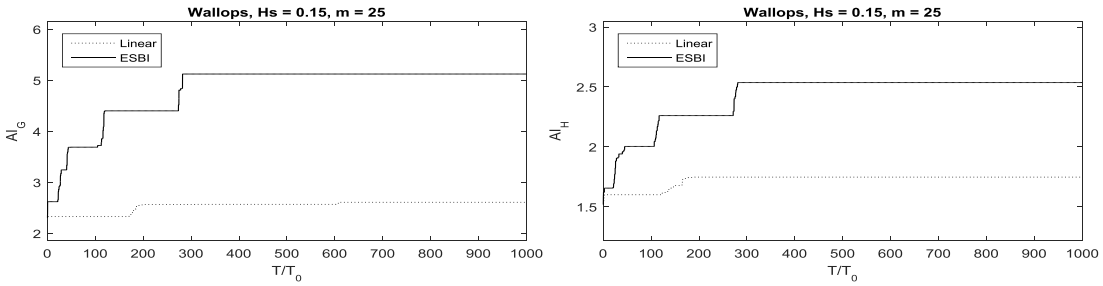

(c) (d)

FIG. 3. The abnormality indexes against time

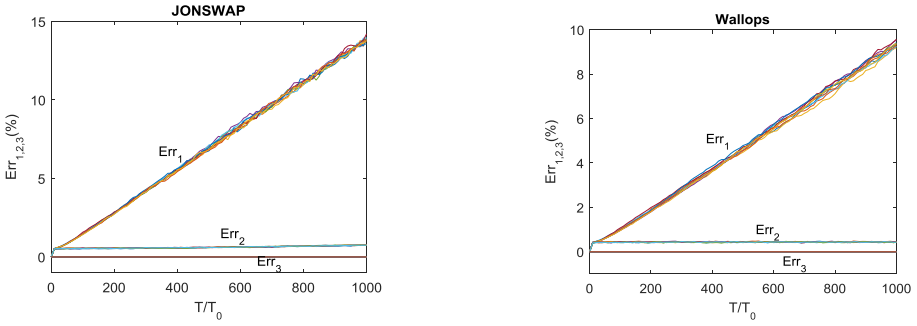

(a) $H_s = 0.01,\ \gamma = 9$ (b) $H_s = 0.01,\ m = 25$

FIG. 4. $Err_{1,2,3}$ against time for different random phases

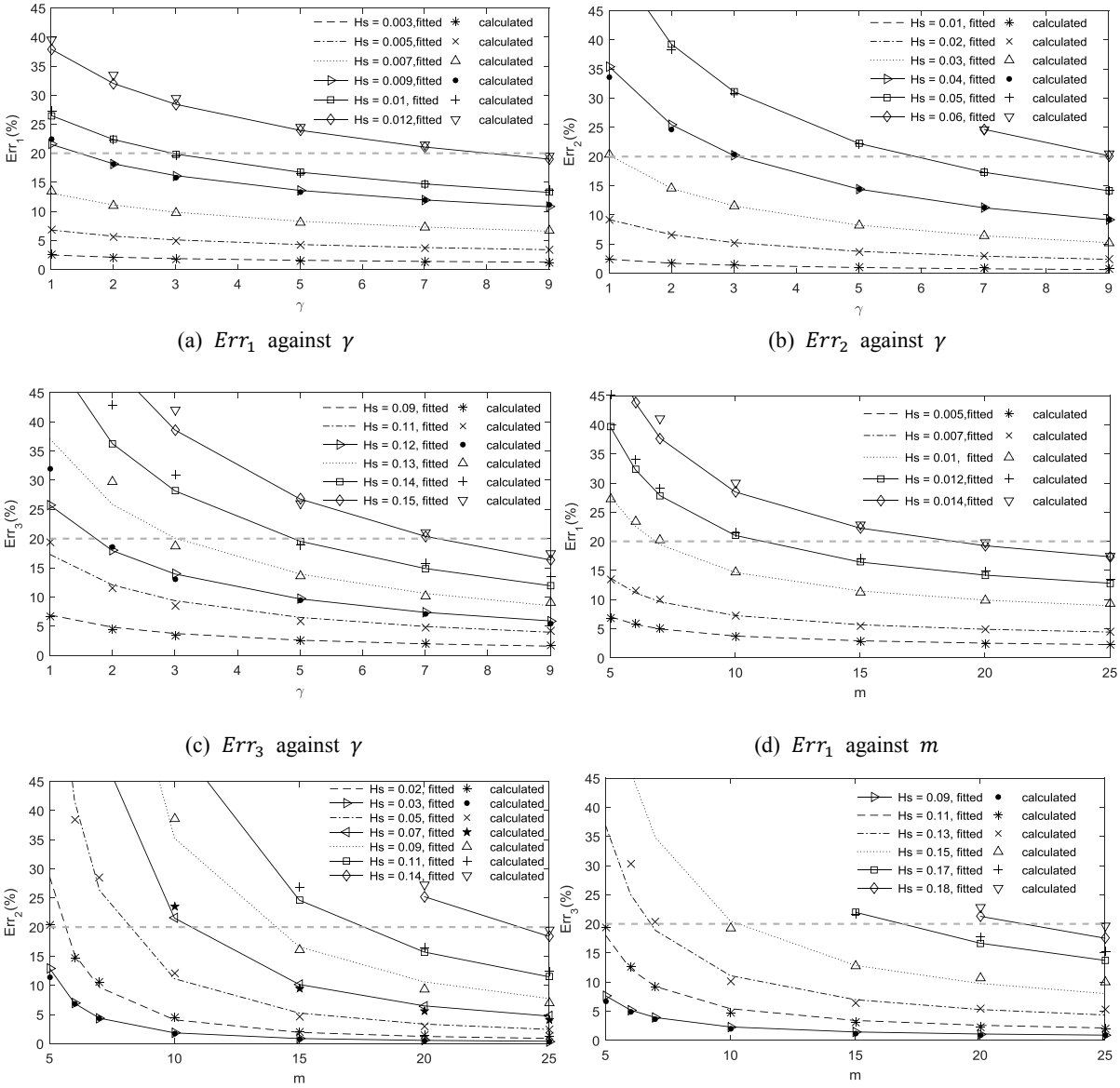

(a) Err_1 against γ

(b) Err_2 against γ

(c) Err_3 against γ

(d) Err_1 against m

(e) Err_2 against m

(f) Err_3 against m

FIG. 5. Calculated and fitted errors of simplified models based on the JONSWAP(a-c) and Wallops(d-f) spectrum

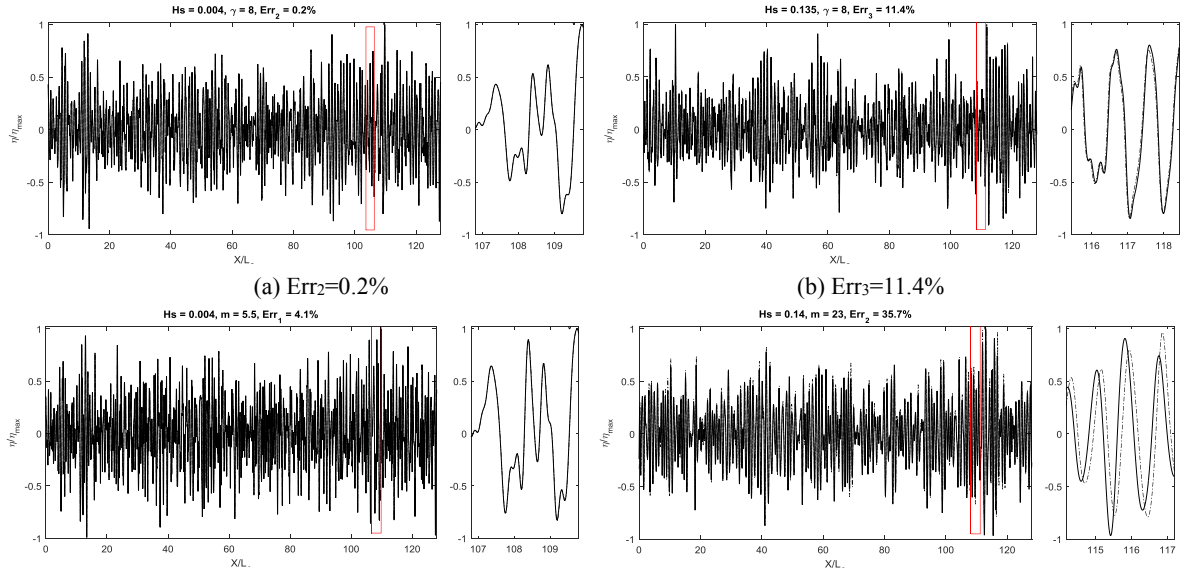

(a) Err$_2$=0.2%

(b) Err$_3$=11.4%

(c) Err_1=4.1% (d) Err_2=35.7%

FIG. 6. Free surface elevation corresponding to different error levels for random phase approach. ('—': ESBI; '-·-·-·': simplified model). (a)(b) for the JONSWAP spectrum and (c)(d) for the Wallops spectrum

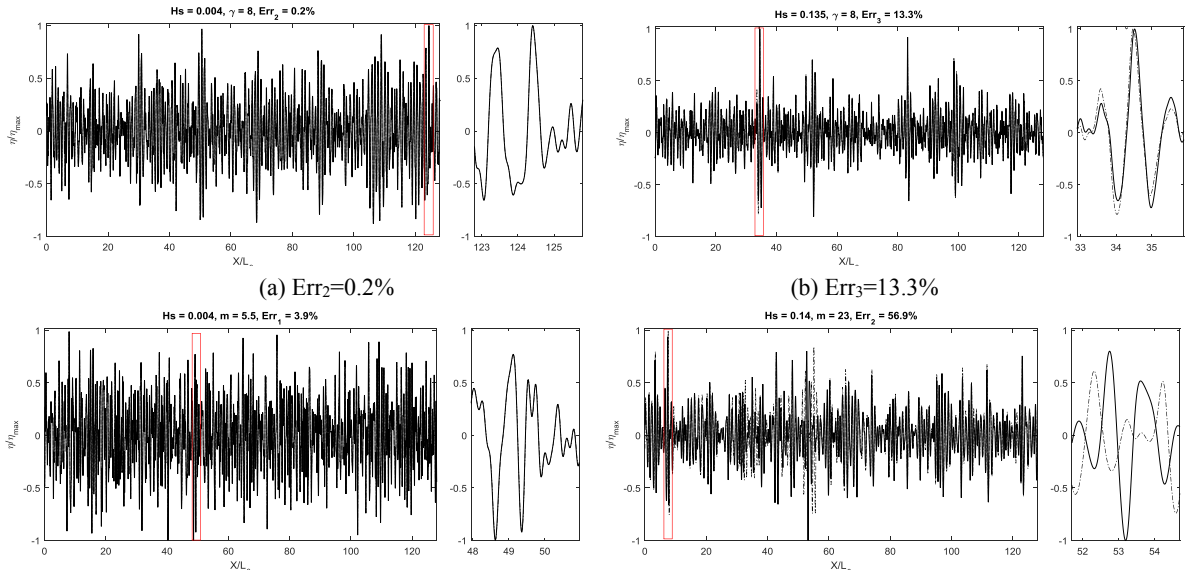

(a) Err_2=0.2% (b) Err_3=13.3%

(c) Err_1=3.9% (d) Err_2=56.9%

FIG. 7. Free surface elevation corresponding to different error levels for random amplitude approach. ('—': ESBI; '-·-·-·': simplified model). (a) (b) for the JONSWAP spectrum and (c)(d) for the Wallops spectrum

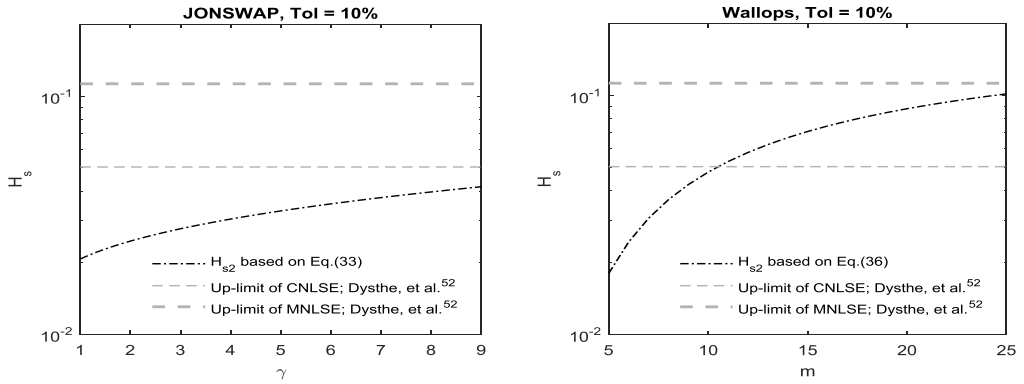

(a) (b)

FIG. 8. Comparison of the maximum significant wave height from Eq. (33) and (36) for ENLSE-5F with estimation of Dysthe, *et al*.[52] for CNLSE and MNLSE

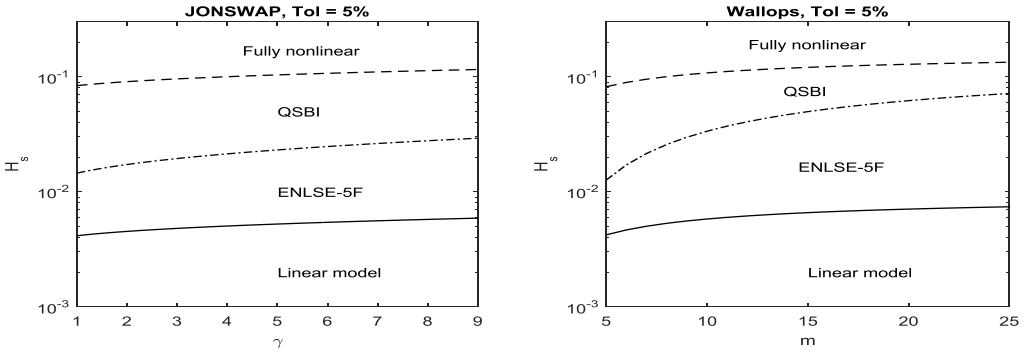

(a) (b)

FIG. 9. Criterion for selecting suitable model ('—': Hs_1, '-.-.-': Hs_2, '----': Hs_3)

Table I. Dimensionless variables

η	Surface elevation multiplied by k_0
$\phi, \tilde{\phi}$	Velocity potential and that at free surface multiplied by $k_0^{3/2}/g^{1/2}$
$\boldsymbol{X} = (X, Y)$	Horizontal space coordinate multiplied by k_0
Z	Vertical space coordinate multiplied by k_0
T	Time coordinate multiplied by ω_0
$\boldsymbol{K} = (\kappa, \zeta), K$	Wave number and its module multiplied by k_0^{-1}
Ω	Wave circular frequency coordinate multiplied by ω_0^{-1}
$\bar{\eta}, A, A_2, A_3$	Free surface coefficients multiplied by k_0
$\bar{\phi}, B, B_2, B_3$	Velocity potential coefficients multiplied by $k_0^{3/2}/g^{1/2}$
H_s	Significant wave height multiplied by k_0
k_j	Wave number of an individual component multiplied by k_0^{-1}
ω_j	Wave circular frequency of an individual component multiplied by ω_0^{-1}
a_j	Wave amplitude of an individual component multiplied by k_0
T_0	Peak period multiplied by ω_0 and equal to 2π

Table II. Summary of the selected unsteady wave models

	Accuracy	Efficiency
Linear model	Satisfactory accuracy for extremely small steepness waves	Most efficient among all
ENLSE-5F	Satisfactory accuracy for small steepness and narrow bandwidth waves, more accurate than linear model	Less efficient than linear model, but faster than the QSBI
QSBI	Satisfactory accuracy for small and moderate steepness waves with any bandwidth, more accurate than ENLSE-5F	Slower than the linear model and ENLSE-5F, but faster than ESBI
ESBI	Satisfactory accuracy for all non-breaking waves, more accurate than QSBI	Most time consuming among all

Table III. Wave parameters for numerical studies

H_s	0.001, 0.003, 0.005, 0.007, 0.009, 0.01, 0.012, 0.014, 0.02, 0.03, 0.04, 0.05, 0.06, 0.07, 0.09, 0.11, 0.12, 0.13, 0.14, 0.15, 0.17, 0.18		
m (Wallops)	5, 6, 7, 10, 15, 20, 25	γ (JONSWAP)	1, 2, 3, 5, 7, 9

Table IV. Average and standard deviation of $Err_{1,2,3}$ for the JONSWAP spectrum

γ	1						9					
	Err1		*Err2*		*Err3*		*Err1*		*Err2*		*Err3*	
H_s	*Avg*	*Std*	*Avg*	*Std*	*Avg*	*Std*	*Avg*	*Std*	*Avg*	*Std*	*Avg*	*Std*
0.01	27.2	0.2	2.3	0.04	9E-4	9E-6	13.9	0.2	0.76	0.01	3E-4	4E-6
0.11	141.7	1.2	114.8	1.7	18.9	1.7	140.0	4.3	55.3	1.4	4.5	0.3

Table V. Average and standard deviation of $Err_{1,2,3}$ for the Wallops spectrum

m	5	25

	Err_1		Err_2		Err_3		Err_1		Err_2		Err_3	
H_s	*Avg*	*Std*	*Avg*	*Std*	*Avg*	*Std*	*Avg*	*Std*	*Avg*	*Std*	*Avg*	*Std*
0.01	27.2	0.2	2.3	0.04	9E-4	9E-6	9.4	0.1	0.4	9E-3	1E-4	4E-6
0.11	141.7	1.2	114.8	1.7	18.9	1.7	138.0	6.9	16.1	1.0	2.34	0.2

Table VI. Comparison between the calculated and predicted error (%) - JONSWAP

γ	1.5						8					
H_s	Err_1	Err_1'	Err_2	Err_2'	Err_3	Err_3'	Err_1	Err_1'	Err_2	Err_2'	Err_3	Err_3'
0.004	3.9	4.0	0.4	0.3	2E-5	4E-6	2.3	2.3	0.2	0.1	7E-6	1E-6
0.015	-	-	4.3	4.4	4E-3	2E-3	-	-	1.6	1.5	1E-3	5E-4
0.06	-	-	-	-	1.0	0.9	-	-	-	-	0.4	0.3
0.135	-	-	-	-	-	-	-	-	-	-	11.4	11.2

Table VII. Comparison between the calculated and predicted error (%) - Wallops

m	5.5						23					
H_s	Err_1	Err_1'	Err_2	Err_2'	Err_3	Err_3'	Err_1	Err_1'	Err_2	Err_2'	Err_3	Err_3'
0.004	4.1	4.1	0.4	0.4	2E-5	1E-5	1.5	1.5	0.2	2E-2	3E-6	2E-6
0.02	-	-	7.8	9.2	1E-2	1E-2	-	-	0.9	0.5	2E-3	2E-3
0.06	-	-	-	-	1.1	1.1	-	-	3.4	3.9	0.2	0.2
0.14	-	-	-	-	-	-	-	-	-	-	7.4	6.4

Table VIII. Comparison between the calculated and predicted errors (%) – JONSWAP (the calculated error is obtained by using the random amplitude approach)

γ	1.5						8					
H_s	Err_1	Err_1'	Err_2	Err_2'	Err_3	Err_3'	Err_1	Err_1'	Err_2	Err_2'	Err_3	Err_3'
0.004	4.0	4.0	0.4	0.3	2E-5	4E-6	2.3	2.3	0.2	0.1	8E-6	1E-6
0.015	-	-	4.3	4.4	4E-3	2E-3	-	-	1.5	1.5	1E-3	5E-4
0.06	-	-	-	-	1.0	0.9	-	-	-	-	0.4	0.3
0.135	-	-	-	-	-	-	-	-	-	-	13.3	11.2

Table IX. Comparison between the target and predicted error (%) – Wallops (the calculated error is obtained by using the random amplitude approach)

m	5.5						23					
H_s	Err_1	Err_1'	Err_2	Err_2'	Err_3	Err_3'	Err_1	Err_1'	Err_2	Err_2'	Err_3	Err_3'
0.004	3.9	4.1	0.4	0.4	2E-5	1E-5	1.5	1.5	0.2	2E-2	3E-6	2E-6
0.02	-	-	8.7	9.2	1E-2	1E-2	-	-	1.0	0.5	3E-3	2E-3
0.06	-	-	-	-	1.0	1.1	-	-	3.6	3.9	0.1	0.2
0.14	-	-	-	-	-	-	-	-	-	-	8.0	6.4